

# Molecular Dynamics in Liquids: Spin-Lattice Relaxation of Nitroxide Spin Labels

Bruce H. Robinson, Duncan A. Haas, Colin Mailer

Time domain pulsed saturation recovery and electron-electron double resonance spectroscopies were used to measure the spin-lattice relaxation rates of the electron and the nitrogen nucleus in nitroxide spin labels in liquids. The rotational correlation time range covered is from picoseconds to milliseconds. These rates are quantitatively explained by isotropic rotational Brownian dynamics, which modulate the interactions between the electron spin and the molecular angular momentum; the nitrogen and electron spins; and the solvent protons with both the electron and the nitrogen spins. This solves a 20-year-old problem that has limited scientific applications of nitroxides.

Nitroxide spin labels have been used as probes of molecular motion in the biological and physical sciences for the past 25 years (1). Electron paramagnetic resonance (EPR), in conjunction with the spin-label methodology, is a very powerful technique for the study of dynamics over a range from picoseconds to milliseconds in rotational correlation times. One uses indirect information, such as spin-lattice relaxation rates ( $T_{1e}^{-1}$ ) or motionally induced changes in spectral line shapes, to make a statement about the dynamics of the system of interest. Continuous wave (CW)-EPR, with use of spectral line widths and slow-motion theory (2), gives information on motion on the picosecond to nanosecond time scale. The technique of CW-saturation transfer (ST)-EPR (3) produces spectra whose shapes are determined by competition among spin relaxation rates, magnetic field modulation, and motional rates in the sub-microsecond regime. Application of line-shape simulation methods to aid data analysis has been limited until recently (4) to relatively simple dynamical models because truly accurate simulations require detailed knowledge of all relaxation processes. Given the ubiquity of EPR spin-label usage in liquids and the existence of well-developed theory (5) for transverse spin-spin relaxation rates ( $T_{2e}^{-1}$ ), it is somewhat surprising that a clear understanding of longitudinal relaxation mechanisms ( $T_{1e}^{-1}$ ) has not emerged until now. We (i) show how both electronic ( $T_{1e}^{-1}$ ) and nuclear ( $T_{1n}^{-1}$ ) spin-lattice relaxation rates can be measured directly and unequivocally and (ii) describe the relation between the molecular dynamics and these experimentally determined relaxation rates.

Relaxation rates are traditionally estimated by CW power saturation: The CW-EPR sig-

nal height, when measured as a function of incident microwave power, rises to a maximum and then decreases. The power level at which the signal is maximum can be related to relaxation rates of the spin. Altenbach *et al.* (6) determined the  $\alpha$ -helical nature of a transmembrane protein from the periodicity of the saturation behavior of spin labels selectively attached to various amino acid side chains in the sequence. The results depended on the collision rate of paramagnetic oxygen being fast enough to shorten the spin-label relaxation rates (and alter the power for maximum signal) for those spin labels that had access to oxygen. This indirect method can be a very powerful way to obtain structural information. However, indirect methods will always raise questions about how the results are influenced by hidden processes, for example, the nature of the translational collision mechanism, the use of magnetic field modulation for signal detection, and the EPR line shapes. Although there is some understanding of how the saturation curves relate to the actual relaxation rates (2), direct measurement of the spin-lattice relaxation rates would remove these concerns.

Our results were obtained by pulsed saturation recovery (SR)-EPR (7) and by SR electron-electron double resonance (SR-ELDOR) (8); these are time domain, polarization-transfer experiments in which the return to equilibrium of a spin system is monitored after a microwave pulse has perturbed the electron polarization. In SR-EPR, the microwave frequency used to observe the recovery is the same as that of the pump; the signal is the return to thermal equilibrium as the polarization spreads throughout the spin system and out to the lattice. In SR-ELDOR, the frequency of the observer is different from that of the pump. Electron spins polarized at the pump frequency transfer energy to the spins at the observe frequency by means of nuclear spin flips (at rate  $T_{1n}^{-1}$ ), which then return to

thermal equilibrium at rate  $T_{1e}^{-1}$  (Fig. 1). The arrival of magnetization (and the relaxation to equilibrium) can be clearly detected (Fig. 2).

Hyde and co-workers pioneered the SR-EPR and SR-ELDOR techniques in liquids. They have applied SR-EPR to a number of systems: nitroxides (9), melanins (10), spin-labeled melittin (11), and membranes (12). Fajer *et al.* (13) attempted to observe motion by its effect on  $T_{1e}^{-1}$  with SR-EPR, and Hornak and Freed (14) used field jump ELDOR, but contributions of nuclear relaxation were not taken into account, making the results equivocal. The difficulties encountered in connecting the relaxation rates to dynamical processes are best summarized by Hyde *et al.* (8): "The existing lack of understanding of electron spin-lattice relaxation mechanisms of nitroxide radical spin labels has again been confirmed and must now be joined by a corresponding lack of understanding of nitrogen nuclear relaxation mechanisms."

We used SR-ELDOR and SR-EPR to measure spin-lattice relaxation rates using 0.5 mM perdeuterated  $^{15}\text{N}$  2,2,6,6-tetramethyl-4-piperidinol-1-oxyl (TEMPOL) in glycerol-water mixtures. The use of the  $^{15}\text{N}$  isotope (nuclear spin  $I = 1/2$ ), which gives two EPR lines (rather than three as does the  $^{14}\text{N}$  isotope with  $I = 1$ ), is important as a means of simplifying the spectra and reducing the number of possible relaxation path-

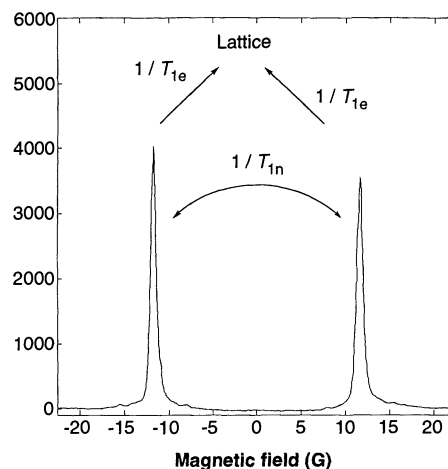
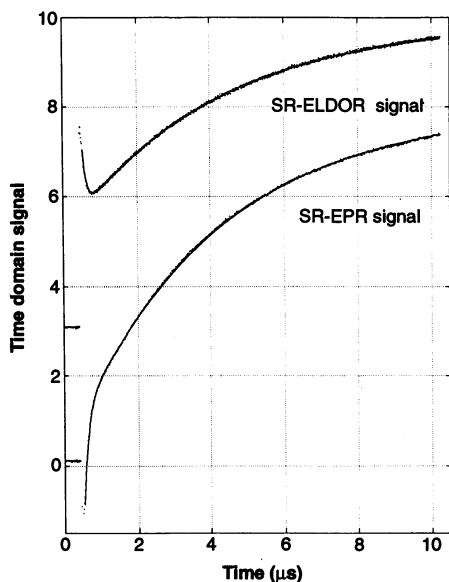


Fig. 1. An experimental CW-EPR absorption spectrum of  $^{15}\text{N}$  TEMPOL (in arbitrary units) showing two individual resonances separated by  $\bar{a}$  (2.25 mT); also indicated are the electron and nuclear spin-lattice relaxation pathways.

Department of Chemistry, University of Washington, Seattle, WA 98195.

ways. The complications of  $T_{1n}^{-1}$  processes have limited the experimental success of saturation recovery pulsed experiments; the sign change of the  $T_{1n}^{-1}$  process in SR-ELDOR (Fig. 2) is an essential requirement for disentangling the  $T_{1e}^{-1}$  and  $T_{1n}^{-1}$  curves. An important requirement is to span a wide range in correlation times, here from 10 ps to 100  $\mu$ s. The correlation times ( $\tau_c$ ) for the spin label in both glycerol-water mixtures and *sec*-butyl benzene were independently determined from the CW-EPR spectra. The Stokes-Einstein equation,  $\tau_c = V(\eta/k_B T)$ , relates the molecular rotational correlation time to the macroscopic parameters of the effective hydrodynamic volume ( $V$ ) of the spin probe, the solvent viscosity ( $\eta$ ), and temperature ( $T$ );  $k_B$  is the Boltzmann constant. Both  $V$  and  $\eta$  are known functions of the temperature and solvent (15).

The 9.3-GHz (X-band) pulsed EPR spectrometer used for these studies follows published designs (16). The pump-observer frequency difference is phase locked to a low-frequency (megahertz) oscillator; experimental operation is simplified by the use of a Medical Advances (Milwaukee, Wisconsin) loop gap resonator (LGR) model XP-0201



**Fig. 2.** Experimental SR-ELDOR and SR-EPR responses (in arbitrary units) of  $^{15}\text{N}$  TEMPOL in 40% glycerol at a  $\tau_c$  of 0.15 ns. For SR-ELDOR, the high-field line was pumped with a 250-mW, 100-ns pulse, and the low-field line was observed with 100  $\mu$ W; dead time, 80 ns; acquisition time, 10 ns per point for 1024 points. The pulse repetition rate was  $\sim 3$  kHz. For SR-EPR, the pump and observer are both set to the low-field line. Superimposed on the data are the least squares best fits, which assume two independent exponential relaxation components and a baseline. The relaxation rates are the same for both data sets:  $T_{1e}^{-1}$  is 0.249 Mrad/s and  $T_{1n}^{-1}$  is 7.507 Mrad/s. The amplitudes of the  $T_{1n}$  decay have opposite signs in the two signals.

instead of a bimodal EPR cavity. The quality factor  $Q$  of the LGR is low enough so that the microwave radio-frequency (rf) field can significantly perturb the spin system at the 60 to 70 MHz offset needed for the SR-ELDOR experiment (17). The small size of the LGR produces a high power density leading to large rf fields for moderate powers (less than 1 W). Individual decay curves were obtained in a few minutes of signal averaging.

### Electron Spin-Lattice Relaxation

There are many spin-relaxation mechanisms described in the literature (18), four of which are important in spin labels. The first is the spin-rotation (sr) interaction in which the angular velocity of the molecule directly relaxes the electron. The second mechanism is the electron-nuclear dipolar (end) interaction in which the electron and the nitrogen nucleus relax each other through a direct magnetic coupling of their spins. The third mechanism is spin diffusion (sd) in which the electron and the nitrogen nucleus are coupled to the protons in the solvent. The fourth is collision-induced Heisenberg exchange by paramagnetic oxygen (ox), whose very short relaxation time relaxes the spin label (19).

The four mechanisms for electron spin-lattice relaxation are statistically independent and do not cross correlate with one another. The total spin-lattice relaxation rate is therefore

$$(T_{1e}^{-1})^{-1} = (T_{1e}^{\text{sr}})^{-1} + (T_{1e}^{\text{end}})^{-1} + (T_{1e}^{\text{sd}})^{-1} + (T_{1e}^{\text{ox}})^{-1} \quad (1)$$

The Hamiltonian for the spin-rotation mechanism, originally introduced by Hubbard (20), shows that the electron spin,  $\mathbf{S}$ , is coupled to the angular momentum,  $\mathbf{J}$ :  $H_{\text{sr}} = \hbar \mathbf{S} \cdot \mathbf{C} \cdot \mathbf{J}$ , where  $\hbar$  is Planck's constant divided by  $2\pi$  and  $\mathbf{C}$  is the coupling tensor. The angular momentum is related to the angular velocity,  $\omega$ , through the inertial tensor,  $\mathbf{I}$ , as  $\hbar \mathbf{J} = \mathbf{I} \cdot \omega$ . Atkins and Kivelson (21) showed that the coupling tensor is related to the spin-field coupling  $\mathbf{G}$  (the G tensor) for the spin probe by  $\mathbf{C} \cdot \mathbf{I} = -\hbar(\mathbf{G} - g_e \mathbf{1})$ , where  $g_e$  is the free-spin G value. One can predict, with fast-motion Redfield theory (22), that the effects of isotropic Brownian rotational motion on this Hamiltonian lead to a relaxation rate of

$$(T_{1e}^{\text{sr}})^{-1} = \frac{\sum_{i=1}^3 (g_i - g_e)^2}{9\tau_c} \quad (2)$$

where  $g_i$  are the eigenvalues of the G tensor.

The second mechanism requires the direct electron-nitrogen dipolar interaction Hamiltonian,  $H_{\text{end}} = \hbar \mathbf{S} \cdot \mathbf{A} \cdot \mathbf{I}$ . The spin of

the electron,  $\mathbf{S}$ , and of the nucleus,  $\mathbf{I}$ , are coupled by the chemical splitting or hyperfine tensor,  $\mathbf{A}$ . We have extended Abragam's treatment for this mechanism to predict a relaxation rate for the electron

$$(T_{1e}^{\text{end}})^{-1} = \frac{1}{6} \sum_{i=1}^3 (a_i - \bar{a})^2 \frac{\tau_c}{1 + (\omega_e \tau_c)^2} \quad (3)$$

where  $a_i$  are the eigenvalues of the hyperfine tensor,  $\bar{a}$  is the average of the eigenvalues, and  $\omega_e$  is the electron Larmor frequency of  $2 \times 10^{11}$  rad/s. Another Hamiltonian—that of the chemical shift anisotropy (csa),  $H_{\text{csa}} = \beta_e \mathbf{H}_0 \cdot \mathbf{G} \cdot \mathbf{S}$ , where  $\beta_e$  is the Bohr magneton—couples the spin to the field,  $\mathbf{H}_0$  through the G tensor. Cross correlation of the csa and the end may lead to a line-position-dependent relaxation rate, which is an important contribution to spin-label line widths ( $T_{2e}$  relaxation). The measured  $T_{1e}^{-1}$  values from both  $^{14}\text{N}$  and  $^{15}\text{N}$  nitroxide spin labels are independent of field position. We therefore conclude that the csa-end cross-correlation contribution to  $T_{1e}^{-1}$  can be neglected.

The third mechanism is spin diffusion, in which the solvent protons are coupled to the electron and the nucleus. The treatment of this effect, originally developed by Kushtville and deGennes, is summarized by Blumberg (23). Spin-diffusion theory states that magnetization can migrate through a proton spin system by means of mutual spin flips. The proton spin-diffusion coefficient,  $D_{\text{sd}}$ , is related to the spin-flip rate,  $W$ , by  $D_{\text{sd}} = 2rW$ , where  $r$  is the mean distance between protons. An electron or a paramagnetic impurity, having a rapid relaxation rate, can relax the magnetization of the solvent protons. We suggest that the converse is also true: The electron magnetization can be relaxed by the bulk solvent. The result is  $(T_{1e}^{\text{sd}})^{-1} = 8.5\rho(CD_{\text{sd}}^3)^{1/4}$ . The density of protons is  $\rho$ , and the effects of the electron-proton interaction modulated by the dynamics are contained in  $C$ .

There exist in the literature several different treatments of the nature of the interaction of a probe molecule with solvated spins modulated by translational motion. One is the Torrey random flight model, which was developed for modulation of the dipolar interaction (24). A similar treatment was carried out by Hunt and Powles (25). Abragam developed a theory for the modulation of the scalar coupling by Heisenberg exchange (22). All methods have a common functional form for  $C$

$$C = \alpha \frac{\tau_d}{1 + (\omega_e \tau_d)^{3/2}}$$

The relative solvent-probe translational diffusion time,  $\tau_d$ , and the rotational correlation time of the spin probe,  $\tau_c$ , are proportional. The proportionality constant is de-

terminated by the relative hydrodynamics mobilities of the solvent and spin probe and, here, is between 0.5 and 3.0. Therefore, it is reasonable to assume that  $\tau_d = \tau_c$ . The very weak power dependence and the small contribution of this mechanism to the overall rate means that the lack of precision of the proportionality constant does not lead to significant errors. Combining the above expressions

$$(T_{1e}^{sd})^{-1} = R_{1e,max}^{sd} \left( \frac{2\omega_e\tau_c}{1 + (\omega_e\tau_c)^2} \right)^{1/4} \quad (4)$$

where  $R_{1e,max}^{sd}$  is the maximum possible relaxation rate, regardless of correlation time, and is an adjustable parameter for the purposes of fitting our experimental data. Unlike all the other terms in the formulae for  $T_{1e}^{-1}$ , the value of  $R_{1e,max}^{sd}$  cannot be calculated from first principles:  $D_{sd}$  is not known and the Hamiltonian is not completely specified.

Additional relaxation occurs because of the presence of oxygen, a paramagnetic relaxation agent. Hyde and Subczynski (19) have reviewed the effects of oxygen and demonstrated that oxygen should increase the spin-label  $T_{1e}^{-1}$  rate by a factor that is proportional to oxygen concentration,  $[O_2]$ , and to the relative spin label-oxygen translational diffusion coefficient. We assume that this translational diffusion coefficient is proportional to the rotational correlation time of the spin label; the proportionality constants are subsumed into  $K_{ox}$ , which is spin-label specific. The oxygen

contribution to the electron spin-lattice relaxation rate is

$$(T_{1e}^{ox})^{-1} = \frac{K_{ox}}{\tau_c} \quad (5)$$

where  $K_{ox}$  is defined as the difference of measured values of  $T_{1e}^{-1}$ , with and without air. We assume that  $[O_2]$  is independent of temperature and percent glycerol, which leads to slight overestimation of the effects of oxygen in the glycerol-water samples.

### Nuclear Spin-Lattice Relaxation

Nuclear spin-lattice relaxation is governed by two mechanisms similar to those for electron relaxation

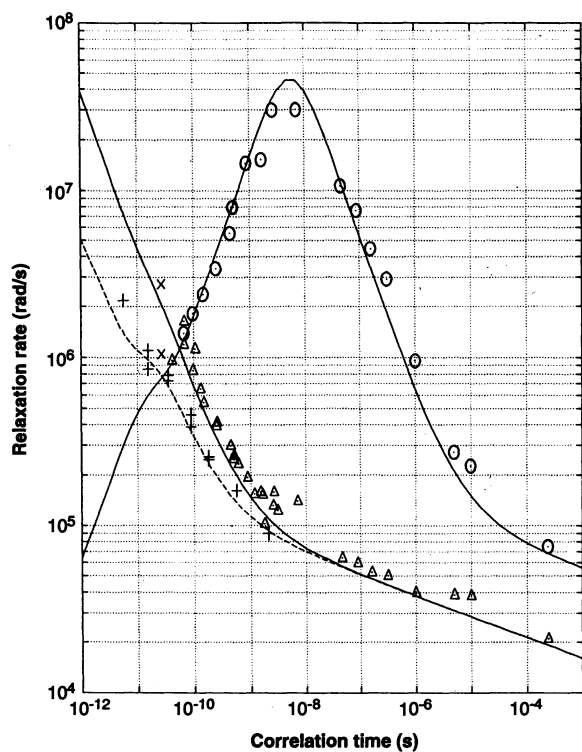
$$(T_{1n})^{-1} = (T_{1n}^{end})^{-1} + (T_{1e}^{sd})^{-1} \quad (6)$$

The electron-nuclear dipolar mechanism for the nitrogen nucleus is almost identical to that for the electron, except that  $\bar{a}I_z S_x$  (along the  $z$  axis) is included in the fluctuations of the interaction Hamiltonian, which leads to an extra term in the relaxation that depends on a frequency  $\omega_a = \bar{a}/2$ . We have

$$(T_{1n}^{end})^{-1} = \frac{1}{20} \sum_{i=1}^3 (a_i - \bar{a})^2 \times \left( \frac{\tau_c}{1 + (\omega_a\tau_c)^2} + \frac{(7/3)\tau_c}{1 + (\omega_e\tau_c)^2} \right) \quad (7)$$

The proton spin-diffusion mechanism is also operative and may be written (by analogy to the electron spin-diffusion relaxation rate) as

**Fig. 3.** Plot of the experimental electron ( $T_{1e}^{-1}$ ) and nitrogen spin-lattice ( $T_{1n}^{-1}$ ) relaxation rates. ( $\Delta$ )  $T_{1e}^{-1}$  and ( $\circ$ )  $T_{1n}^{-1}$  of air-saturated perdeuterated  $^{15}\text{N}$  TEMPOL in glycerol-water mixtures; ( $\times$ )  $T_{1e}^{-1}$  of oxygenated and deoxygenated perdeuterated  $^{15}\text{N}$  TEMPOL in water; and (+)  $T_{1e}^{-1}$  of oxygen-free  $^{15}\text{N}$  TEMPOL in *sec*-butyl benzene, taken from Percival and Hyde (9). The solid lines are the theoretical prediction for  $T_{1e}^{-1}$  (including the oxygen effect) and  $T_{1n}^{-1}$ . The dashed line is the theoretical prediction for  $T_{1e}^{-1}$  excluding the oxygen effect. The eigenvalues of the hyperfine tensor,  $a_i$ , in millitesla, are {0.8, 0.6, 4.675}; the eigenvalues of the  $g$  tensor,  $g_i$ , are {2.0088, 2.0054, 2.0022};  $g_e$  is the free-spin  $g$  value of 2.0023;  $R_{1e,max}^{sd} = R_{1n,max}^{sd} = 0.13$  Mrad/s; and  $K_{ox} = 3 \times 10^{-5}$ .



$$(T_{1n}^{sd})^{-1} = R_{1n,max}^{sd} \left( \frac{2\omega_n\tau_c}{1 + (\omega_n\tau_c)^2} \right)^{1/4} \quad (8)$$

where  $\omega_n$  is the nitrogen nuclear resonance frequency (8.9 Mrad/s) and the maximum nuclear relaxation rate,  $R_{1n,max}^{sd}$ , is obtained from experiment in the same way as its electron counterpart.

### Results and Discussion

Experimental SR-EPR and SR-ELDOR spin-lattice relaxation signals are illustrated in Fig. 2. The change in sign of the component with the faster relaxation rate shows that this component arises from magnetization transfer between the nuclear manifolds with a relaxation rate  $(T_{1n}^{-1} + T_{1e}^{-1})$ . The two signals are pooled, that is, both data sets are fit to a model that is the sum of two exponentials plus a baseline. The rates of the two exponentials are the same for both the SR-EPR and the SR-ELDOR signals, but the amplitudes of the two components can be different in magnitude and sign. This is an application of global analysis, an approach commonly used in optical spectroscopy (26). At motional times longer than  $\tau_c \sim 100$  ns, additional exponentially decaying components must be included in the analysis (27). Figure 3 shows the experimentally and theoretically determined values of  $T_{1e}^{-1}$  and  $T_{1n}^{-1}$  plotted as functions of the correlation time. The samples were air-saturated perdeuterated  $^{15}\text{N}$  TEMPOL in glycerol-water mixtures. Also plotted are data from oxygen-free  $^{15}\text{N}$  TEMPOL in *sec*-butyl benzene taken from the 1976 experiments of Percival and Hyde (9). The two data points at a correlation time of  $2.6 \times 10^{-11}$  s ( $\times$ ) are the  $T_{1e}^{-1}$  of perdeuterated  $^{15}\text{N}$  TEMPOL in oxygenated and oxygen-free water. The drop in  $T_{1e}^{-1}$  (from 2.5 to 1.1 Mrad/s) was used to estimate  $K_{ox} = 3.3 \times 10^{-5}$ ; using CW-EPR techniques, Hyde and Subczynski (19) determined that  $K_{ox} \approx 3 \times 10^{-5}$ . The theoretical curves of  $T_{1e}^{-1}$  and  $T_{1n}^{-1}$  for the oxygenated samples (solid lines in Fig. 3) were calculated with the known magnetic  $\mathbf{A}$  and  $\mathbf{G}$  tensors and  $K_{ox}$ . The  $T_{1e}^{-1}$  curve was also calculated with the same parameters but without the oxygen contribution to the relaxation (dashed line in Fig. 3). The only adjustable parameters were  $R_{1e,max}^{sd}$  and  $R_{1n,max}^{sd}$ ; both have the same value obtained independently from the data in the microsecond correlation time regime.

The oxygenated glycerol-water  $T_{1e}^{-1}$  and  $T_{1n}^{-1}$  spin-label data and the oxygen-free  $T_{1e}^{-1}$  data for the same spin label in *sec*-butyl benzene fit the same theory (Fig. 3). The high quality of the agreement between theory and experiment suggests that no additional spin interactions have much significance. The complicated dependence of  $T_{1e}^{-1}$  on  $\tau_c$  is a result of the need to add up the

contributions of different mechanisms, each being very simple and peaking at different correlation times. Theory and experiment show that nitroxide spin labels are in the unusual situation of having nuclear relaxation much faster than electron relaxation. This is because the electron is a more efficient relaxing agent than the weaker nuclear spin. From the theory, it is now possible to predict  $T_{1e}^{-1}$  at any spectrometer frequency. We have recently explained the 1- to 18-GHz frequency dependence of the  $T_{1e}^{-1}$ 's of spin-labeled lipids showing that the motion is anisotropic (28, 29).

The theoretical maximum of  $T_{1n}^{-1}$  is  $\sim 45$  Mrad/s, but the experimental values are  $\sim 30$  Mrad/s (Fig. 3). When a theoretical prediction of a relaxation rate is too small, it can be assumed that additional mechanisms need to be considered. However, when a theoretical estimate is larger than the experimental rate, then the theory must be incomplete. The  $T_{1n}^{-1}$  data are not band limited by the spectrometer because 100-Mrad/s rates can be measured. The discrepancy arises from the neglect of higher order terms in the  $(T_{1n}^{\text{end}})^{-1}$  Hamiltonian. Full computer simulation (30) puts the theory for  $T_{1n}^{-1}$  in excellent agreement with experiment and shows that the simpler fast-motion theory overestimates the relaxation rate by  $\sim 25\%$  (but only in the region of the maximum).

Consider now the dependence of  $T_{1e}^{-1}$  on correlation times when  $\tau_c$  is more than a microsecond. Experimentally, we find that  $T_{1e}^{-1}$  is proportional to  $\tau_c^{-1/8}$ . Such a power law has also been observed by Fajer *et al.* (13) in a slow-motion study of spin-labeled hemoglobin. This weak power-law dependence of relaxation rates on motion in very viscous media has been suggested for protons in the nuclear magnetic resonance (NMR) literature and is attributed to translational motion and spin diffusion in liquids (31). We believe that this same mechanism applies to the relaxation of the electron. Translational motion could be modulating either the dipole-dipole or the (scalar) exchange coupling between the electron and solvent spins. Our finding that the maximum relaxation rates for both the nitrogen nucleus ( $R_{1n,\text{max}}^{\text{sd}}$ ) and the electron ( $R_{1e,\text{max}}^{\text{sd}}$ ) are the same is inconsistent with a dipolar mechanism (which predicts they should differ by a factor of 5). Modulation of the exchange coupling is independent of the gyromagnetic ratio of the spin species being relaxed and is therefore a better candidate.

## Conclusions

Two motional mechanisms have been invoked to explain the spin lattice relaxation rates over eight orders of magnitude in motion. They are the simplest possible: isotropic Brownian rotational motion and

isotropic Brownian translational motion. Rotational motion in combination with the spin-rotation and the electron-nuclear-dipolar Hamiltonians explains the spin rotation and electron-nuclear relaxation rates. Translational motion plus appropriate Hamiltonians explains the spin diffusion and oxygen contributions to  $T_{1e}^{-1}$ . This explanation is very simple in structure and makes use of standard fast-motion Redfield theory (22) to predict the relaxation rates. It is in accord with standard NMR theory, where such mechanisms and spectral density functions are well documented. A sum of the mechanisms explains both spin-lattice electron relaxation and spin-lattice nuclear relaxation. Only one constant has had to be set to bring the entire theory into agreement with the data.

This combination of theory and experiment explains electron relaxation in liquids in which the viscosity varies from that of room-temperature water to a value more than  $10^7$  times greater. Over this enormous range, the relaxation rates are sensitive, nontrivial, and continuous functions of the correlation time. With no additional adjustable numbers, we have not only explained our own data but also that of Percival and Hyde (9) on the same spin label in a different solvent  $100^\circ\text{C}$  colder than our experiments. Even at very high viscosities, the relaxation processes are dominated by liquid mechanisms. At some point, as the temperature is lowered and the viscosity increases further, classical EPR solid relaxation mechanisms must come into play and dominate the relaxation (32), but over the temperature range of our investigations, there is no evidence for them.

The future of applications of pulsed EPR techniques to a variety of problems is very promising. The theory has already successfully elucidated anisotropic motion of lipids (28, 29) and can be applied to other systems with equal ease. The measured values of the spin-lattice relaxation rates provide data previously not available for detailed line-shape simulations used to extract motional processes. The "CW saturation roll-over" method of extracting spin-lattice relaxation rates can be complemented by direct measurement of the rates. Pulsed EPR is a straightforward alternative to standard CW-EPR for measurement of rotational correlation times. That both  $T_{1e}^{-1}$  and  $T_{1n}^{-1}$  are sensitive, independent functions of the correlation time means that these numbers can now be directly used to extract motional information over the entire continuous range from picoseconds to milliseconds. That a single technique can cover such a wide dynamic range is exceptional. This methodology may be used to study a dynamics process in which the dynamic models are of arbitrary complexity.

## REFERENCES AND NOTES

1. L. J. Berliner, Ed., *Spin Labeling: Theory and Applications* (Academic Press, New York, 1976 and 1979), vols. I and II; \_\_\_\_\_ and J. Reuben, Eds., *Biological Magnetic Resonance* (Plenum, New York, 1989), vol. 8.
2. D. A. Haas, C. Mailer, B. H. Robinson, *Biophys. J.* **64**, 594 (1993).
3. J. S. Hyde and L. R. Dalton, in *Spin Labeling: Theory and Applications*, L. J. Berliner, Ed. (Academic Press, New York, 1979), vol. 2, chap. 1.
4. B. H. Robinson, L. J. Slutsky, F. P. Auteri, *J. Chem. Phys.* **96**, 2609 (1992).
5. J. S. Hwang, R. Mason, L. P. Hwang, J. H. Freed, *J. Phys. Chem.* **79**, 489 (1975).
6. C. Altenbach, T. Marti, H. G. Khorana, W. L. Hubbell, *Science* **248**, 1088 (1990).
7. M. Huisjen and J. S. Hyde, *Rev. Sci. Instrum.* **45**, 669 (1974).
8. J. S. Hyde, W. Froncisz, C. Mottley, *Chem. Phys. Lett.* **110**, 621 (1984).
9. P. W. Percival and J. S. Hyde, *J. Magn. Reson.* **23**, 249 (1976).
10. T. Sarna and J. S. Hyde, *J. Chem. Phys.* **69**, 1945 (1978).
11. C. Altenbach, W. Froncisz, J. S. Hyde, W. L. Hubbell, *Biophys. J.* **56**, 1183 (1989).
12. J. B. Feix *et al.*, *Biochemistry* **23**, 2293 (1984).
13. P. Fajer, D. D. Thomas, J. B. Feix, J. S. Hyde, *Biophys. J.* **50**, 1195 (1986).
14. J. P. Hornak and J. H. Freed, *Chem. Phys. Lett.* **101**, 115 (1983).
15. D. A. Haas, thesis, University of Washington (1993).
16. C. Mailer, D. A. Haas, E. J. Hustedt, J. G. Gladden, B. H. Robinson, *J. Magn. Reson.* **91**, 475 (1991).
17. C. Mailer, D. A. Haas, B. H. Robinson, *Bull. Magn. Reson.* **14**, 30 (1992).
18. J. H. Freed, in *Multiple Electron Resonance Spectroscopy*, M. M. Dorio and J. H. Freed, Eds. (Plenum, New York, 1979), chap. 3, table 2, pp. 112-113.
19. J. S. Hyde and W. K. Subczynski, in *Biological Magnetic Resonance*, L. J. Berliner and J. Reuben, Eds. (Plenum, New York, 1989), vol. 8, chap. 8, p. 399.
20. P. S. Hubbard, *Phys. Rev.* **131**, 1155 (1963).
21. P. W. Atkins and D. Kivelson, *J. Chem. Phys.* **44**, 169 (1966).
22. A. Abragam, *The Principles of Nuclear Magnetism* (Oxford Univ. Press, London, 1961), chap. 8.
23. W. E. Blumberg, *Phys. Rev.* **119**, 79 (1960).
24. H. C. Torrey, *ibid.* **92**, 962 (1953).
25. B. I. Hunt and J. G. Powles, *Proc. Phys. Soc. London* **88**, 513 (1966).
26. M. Beecham, E. Gratton, M. Ameloot, J. R. Knutson, L. Brand, in *Fluorescence Spectroscopy: Principles*, J. R. Lakowicz, Ed. (Plenum, New York, 1991), vol. 2, chap. 5.
27. D. A. Haas, C. Mailer, T. Sugano, B. H. Robinson, *J. Phys. Chem.* **97**, 2914 (1993).
28. J. J. Yin and J. S. Hyde, *Multifrequency Saturation Recovery*, poster 124 of the EPR Symposium at the 34th Rocky Mountain International Conference on Analytical Chemistry, Denver, CO, 2 to 6 August 1992.
29. B. H. Robinson, C. Mailer, J. J. Yin, J. S. Hyde, *Anisotropic Motion in Spin-Labeled Lipids Studied by Multifrequency Saturation Recovery EPR*, poster 126 of the EPR Symposium at the 35th Rocky Mountain International Conference on Analytical Chemistry, Denver, CO, 25 to 29 July 1993.
30. T. Sugano, thesis, University of Washington (1987), p. 283.
31. D. W. Larsen and S. B. Ranavavare, *J. Phys. Chem.* **88**, 4015 (1984).
32. B. H. Robinson, H. Thomann, A. H. Beth, P. Fajer, L. R. Dalton, in *EPR and Advanced EPR Studies of Biological Systems*, L. R. Dalton, Ed. (CRC Press, Boca Raton, FL, 1985), p. 192.
33. This work was supported by the National Institutes of Health (GM-32681), by a Royalty Research Fund award from the University of Washington, and by the Natural Sciences and Engineering Research Council of Canada.